Microfluidics and Nanofluidics (2018) 22:130
https://doi.org/10.1007/s10404-018-2153-2

RESEARCH PAPER

An efficient micromixer actuated by induced-charge electroosmosis using asymmetrical floating electrodes

Kailiang Zhang[1] · Yukun Ren[1,2,3] · Likai Hou[1] · Xiangsong Feng[1] · Xiaoming Chen[1] · Hongyuan Jiang[1,2]

Received: 6 July 2018 / Accepted: 24 October 2018 / Published online: 1 November 2018

Abstract

Efficient microfluid mixing is an important process for various microfluidic-based biological and chemical reactions. Herein we propose an efficient micromixer actuated by induced-charge electroosmosis (ICEO). The microchannel of this device is easy to fabricate for its simple straight channel structure. Importantly, unlike previous design featuring complicated three-dimensional conducting posts, we utilize the simpler asymmetrical planar floating-electrodes to induce asymmetrical microvortices. For evaluating the mixing performance of this micromixer, we conducted a series of simulations and experiments. The mixing performance was quantified using the mixing index, specifically, the mixing efficiency can reach 94.7% at a flow rate of 1500 μm/s under a sinusoidal wave with a peak voltage of 14 V and a frequency of 400 Hz. Finally, we compared this micromixer with different micromixing devices using a comparative mixing index, demonstrating that this micromixer remains competitive among these existing designs. Therefore, the method proposed herein can offer a simple solution for efficient fluids mixing in microfluidic systems.

Keywords Induced-charge electroosmosis · Micromixing · Asymmetrical floating-electrodes · Asymmetrical microvortices · Comparative mixing index

1 Introduction

Rapid and efficient micromixing of fluids, one of the key functions in microfluidic chips, can facilitate a wide variety of applications, such as biochemical reactions (Xie et al. 2012), drug discovery (Ozcelik et al. 2014; Yesiloz et al. 2017) and medical diagnostics (Gorkin et al. 2010; Ickmans et al. 2013; Lu et al. 2013). For microfluids, it is usually difficult to achieve effective micromixing merely using straight microchannel or without perturbance from external fields as the laminar flow condition in microchannels. To rapidly and efficiently mix fluids in these applications, lots of passive methods (Feng et al. 2013, 2014; Jegatheeswaran et al. 2017), and active ones (Chang and Yang 2007; Matsubara and Narumi 2016) have been studied. Specifically, the passive approaches do not consume external energy but they are strictly restricted by the geometry of microchannels and flow conditions (Xia et al. 2005, 2010; Yasui et al. 2011). Compared to the passive methods, the active ones only need simple channel structure and can be flexibly manipulated by external acoustic, magnetic, or electric field. For external-fields-based methods, acoustically controlled micromixing is non-invasive and flexible, but the acoustic generators are

This article is part of the topical collection "2018 International Conference of Microfluidics, Nanofluidics and Lab-on-a-Chip, Beijing, China" guest edited by Guoqing Hu, Ting Si and Zhaomiao Liu.

Electronic supplementary material The online version of this article (https://doi.org/10.1007/s10404-018-2153-2) contains supplementary material, which is available to authorized users.

✉ Yukun Ren
rykhit@hit.edu.cn

✉ Hongyuan Jiang
jhy_hit@hit.edu.cn

[1] School of Mechatronics Engineering, Harbin Institute of Technology, West Da-zhi Street 92, Harbin 150001, Heilongjiang, People's Republic of China

[2] State Key Laboratory of Robotics and System, Harbin Institute of Technology, West Da-zhi Street 92, Harbin 150001, Heilongjiang, People's Republic of China

[3] The State Key Laboratory of Nonlinear Mechanics (LNM), Institute of Mechanics, Chinese Academy of Science, Beijing 100190, People's Republic of China

expensive and time-consuming for fabrication (Johansson et al. 2009; Ye et al. 2009). Although the magnetic force is useful and powerful for fluid mixing, the applications are confined by the magnetism of fluids, and complicated magnetic moving parts are usually required (Zhou et al. 2015; Zhu and Nguyen 2012).

Recently, electrokinetic micromixing has become increasingly attractive for its simplicity, no moving parts and ease of integration with microelectrodes (Chang and Yang 2007; Chen and Yang 2007; Chiu et al. 2012). The mixing mechanisms of electrokinetic micromixers mainly include AC electroosmotic flow (ACEO) (Sasaki et al. 2006), AC electrothermal flow (ACET) (Wu et al. 2017) and induced-charge electroosmotic flow (ICEO) (Liu et al. 2017; Ren et al. 2017). In these methods, the fluid convection and interfacial perturbation are enhanced by induced microvortices. Importantly, the configurations and locations of microvortices, relying on the arrangement of electrodes, can significantly influence the mixing performance. Since the induced-charge electroosmotic microvortices can flexibly appear where the floating electrode(s) is specifically arranged (Jain et al. 2009; Wu and Li 2008), the ICEO is a promising way for efficient microfluid mixing among these electrically controlled mixing schemes.

Regarding ICEO micromixing, several micromixers so far have been reported (Daghighi and Li 2013; Kai et al. 2012). According to the position of induced vortices relative to the fluid interface, typically, two mixing strategies can be found: the micromixers with vortices crossing fluid interface and the ones with vortices nonintersecting with fluid interface. It has been proved that the former one showed a better performance for the induced vortices with a more intense disturbance on the interface (Harnett et al. 2008). Thereby, for improving the mixing performance, it is useful to generate the vortices intersecting with fluid interface. In previous studies, many researchers employed an array of conducting-posts with various shapes, which are asymmetrically arranged within microchannels to generate the vortices crossing the fluid interface (Harnett et al. 2008; Zhao and Bau 2007). Whereas these three-dimensional conducting-posts often need complicated configuration optimization, and the optimized conducting posts are usually difficult for fabrication (Alipanahrostami and Ramiar 2017; Jain et al. 2009). To design an induced-charge electroosmotic micromixer having simple structure and asymmetrical induced vortices, Wu et al. (2016) proposed a mixing device using the ITO glass with specific electrode structure to replace the complicated conducting posts. Whereas the asymmetrical vortices crossing the fluid interface are generated by applying complicated biased AC signals on the floating-electrodes. This device needs complex control signal to achieve a perfect mixing condition. Apparently, it will be better if we can make an ICEO-actuated micromixer with the advantages of easy fabrication, simple driving signal and dramatic interfacial perturbation.

In this paper, we propose an efficient ICEO-based micromixer containing a polydimethylsiloxane (PDMS)-made microchannel and an Indium Tin Oxide (ITO) glass substrate (Fig. 1a, b). The microchannel is easy to fabricate as its simple straight structure. Importantly, for improving the fluidic interfacial perturbation, six rectangular floating-electrodes are asymmetrically arranged in the main channel to generate vortex pairs that cross the fluid interface (Fig. 1c). And the electrode structure can be conveniently obtained by a mature soft lithography technology. We thoroughly studied the influences of peak voltage, frequency of AC signal, type of AC signal, axial fluid velocity, fluid conductivity and fluid viscosity on the mixing performance of this micromixer. The efficient mixing performance of 94.7% proves that our micromixer can provide a new simple and flexible approach for efficient mixing of fluids with broad applications in microfluidic systems (whole chip is shown in Fig. 1d).

2 Mixing mechanism

The tangential electric field causes the lateral convection of microfluid, then the convection of fluid improves the mixing of samples. Therefore, the basic theory contains three parts.

Electric field The electric potential in the liquid meets the Laplace's equation:

$$\nabla \cdot (\sigma \boldsymbol{E}) = -\sigma \nabla^2 \phi \tag{1}$$

where $\boldsymbol{E}$ is electric filed intensity, ϕ is bulk potential, σ is conductivity of the liquid.

The Laplace equation is subjected to the following boundary conditions:

(1) The potential of the left driving-electrode and the right driving-electrode are,

$$\begin{cases} \widetilde{\phi}_{\mathrm{L}} = V_1 \\ \widetilde{\phi}_{\mathrm{R}} = 0 \end{cases}. \tag{2}$$

(2) At the electrolyte/double layer interface, the RC charging equation provides the required interfacial jump condition, which is,

$$\sigma \cdot \boldsymbol{n} \nabla \widetilde{\phi} = j\omega C_0 (\widetilde{\phi} - \widetilde{\phi}_0) \tag{3}$$

where $\boldsymbol{n}$ is the unit normal vector at the electrode's surface. $\omega = 2\pi f$ is angular field frequency, f is linear frequency, $\widetilde{\phi}$ is the potential in the bulk just outside the electric double layer, $\widetilde{\phi}_0$ is the induced potential of floating electrodes, which is determined by the average potential of the linear domain close to the outer layer of the electric double layer, that is, $\phi_0 = \oint_S \phi(r)\,\mathrm{d}r/S$, S is the surface area of the floating

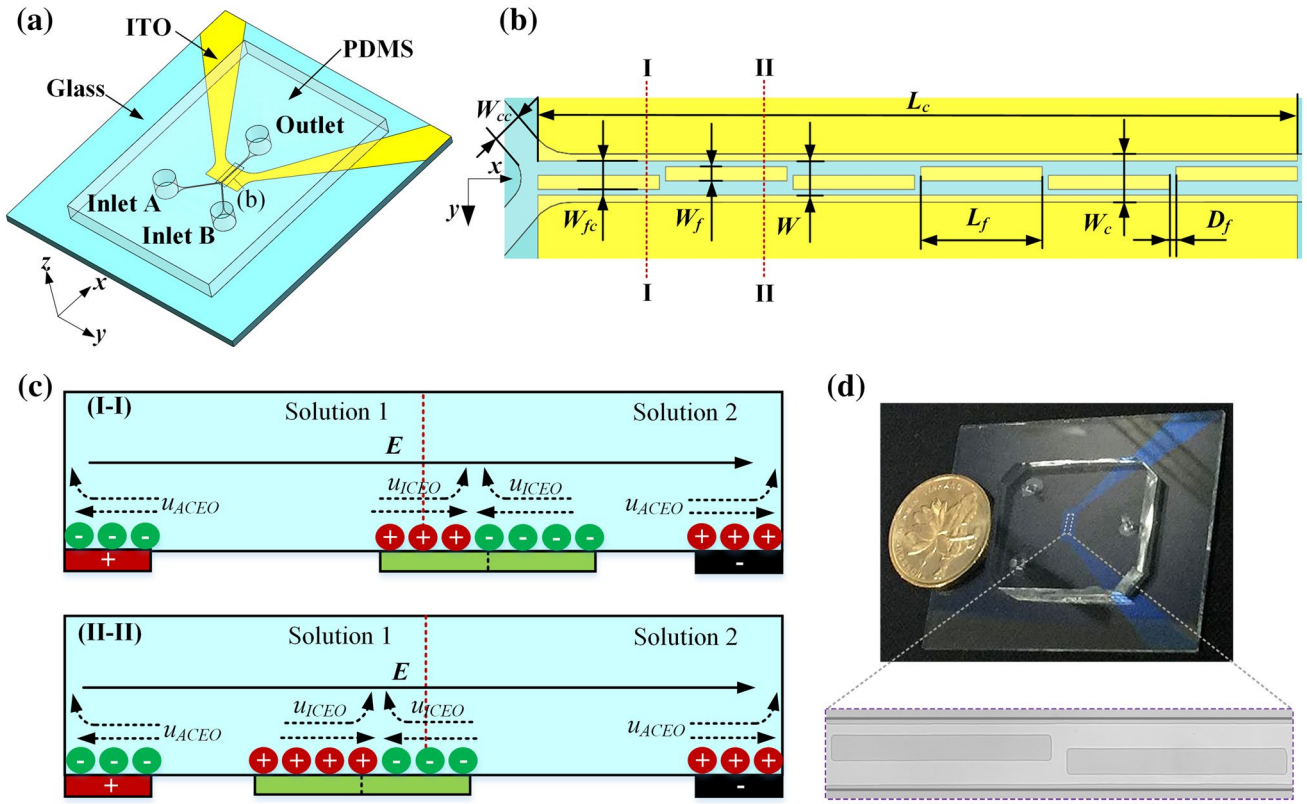

Fig. 1 **a** Schematic diagram of the electro-fluidic device for on-chip fluids mixing. **b** The top view of the main channel, six floating-electrodes are asymmetrically arranged. **c** The principle of fluid flow on the cross-sections of the channel (cross-sections, I–I, II–II, are defined in **b**). **d** A photograph of the micromixer

electrode. $C_0 = C_s C_d/(C_s + C_d)$ is the capacitance of per unit area of the whole induced double layer.

(3) The channel wall meets the following equation:

$$\boldsymbol{n} \cdot \nabla \phi = 0. \tag{4}$$

Flow field According to the Helmholtz–Smoluchowski equation, the induced-charge electroosmotic velocity meets the following equation.

$$\boldsymbol{u}_{\text{slip}} = -\frac{\varepsilon \zeta \boldsymbol{E}_t}{\eta} \tag{5}$$

where ε is the permittivity of fluids, ζ is the potential difference of the electric double layer, η is the viscosity of fluids and $\boldsymbol{E}_t$ is the tangential electric field in the fluids.

A fraction of the double-layer voltage drops across the diffuse layer, acting as the effective induced zeta potential that contributes to ICEO:

$$\widetilde{v} = \frac{1}{1+\delta}(\tilde{\phi}_0 - \tilde{\phi}). \tag{6}$$

Due to appreciable double-layer charging in a low field frequency, the tangential electric field component $\boldsymbol{E}_t = \text{Re}((\tilde{\boldsymbol{E}} - \tilde{\boldsymbol{E}} \cdot \boldsymbol{n} \cdot \boldsymbol{n}) e^{j\omega t})$ at the outer edge of Debye layer exerts Coulomb force on the excessive counterions within the diffuse screening cloud, producing time-averaged nonlinear electroosmotic slip velocity within each AC period:

$$\langle \boldsymbol{u}_{\text{slip}} \rangle = \frac{\varepsilon}{2\eta(1+\delta)} \text{Re}((\widetilde{\phi} - \widetilde{\phi}_0)(\boldsymbol{E} - \boldsymbol{E} \cdot \boldsymbol{n} \cdot \boldsymbol{n})^*). \tag{7}$$

To calculate the bulk ICEO flow field, Eq. (7) is substituted into the following full Stokes equation, as a boundary condition expressing effective electroosmotic slip on the ideally polarizable surface:

$$\nabla \cdot \boldsymbol{u} = 0 \tag{8a}$$

$$-\nabla p + \eta \nabla^2 \boldsymbol{u} = 0. \tag{8b}$$

Concentration field Assuming the electrophoretic effect is neglected, the mass transfer equation can be written as

$$\frac{\partial c}{\partial t} + (v \cdot \nabla) c = \nabla \cdot (D \nabla c) \tag{9}$$

where c is the concentration. The boundary conditions: the concentration values are initially set as 0 and 1 at the two inlets respectively, the channel walls and outlet specified as $\boldsymbol{n} \cdot (-D \nabla c) = 0$.

3 Materials and methods

3.1 Device design and fabrication

This micromixer contains a Y-shaped microchannel (90°) and a transparent ITO glass with specific electrode structure (Fig. 1a). The electrodes extending out of the main channel are the driving electrodes, and the ones arranged in the main channel are the floating electrodes (Fig. 1b). The microchannel has a width of W_c, a length of L_c and a height of H. The driving electrodes have a distance of W, and the width and the length of the floating electrodes are W_f andL_f, respectively. The gap size of the floating electrodes is D_f. All these characteristic dimensions have been marked in Fig. 1b. The specific dimensions of the chip adopted in this study are listed in Table 1.

The fabrication process of this chip mainly includes three steps. The first step is to make a mould with a height of 38 μm by soft lithography using negative dry-film photoresist (RISTON SD238, DUPONT, USA), and the microchannel is obtained by casting and curing PDMS on the mould. The next step is to make the specific electrode structure on ITO glass by soft lithography using positive photoresist AZ4620. Finally, the whole chip is finished by aligning and bonding the PDMS channel and the ITO substrate together using the oxygen plasma treatment.

3.2 Experimental setup

The mixing of an undyed solution and a dyed one has been widely used to evaluate the mixing performance of micromixers. Herein, we use the fluorescein (Kermel Tianjin) as the fluorescent dye for the mixing process visualization. During the experimental process, the fluids are KCl solutions with the same conductivity (0.001 S/m, 0.01 S/m or 0.02 S/m), one labeled with fluorescence, the other without the dye. Finally, the two solutions are simultaneously injected into the main channel of the micromixer through two inlets using a syringe pump (PHD Ultra, Harvard Apparatus). Flow fields are observed using a fluorescence microscope (IX73, Olympus) with a CCD camera (Prime 95B). The AC signal is applied to the driving electrodes using a function generator (TGA12104, TTi). The gray-value of the experimental pictures is measured using an image J software.

4 Results and discussion

4.1 Numerical analysis

According to the basic theories in Sect. 2, we established a numerical simulation model using a commercial software (COMSOL 5.3). The simulation results in Fig. 2a1–a3 show that the fluids with an axial velocity of 1500 μm/s cannot be mixed well only by the molecular diffusion process. Figure 2a4 indicates that the fluids are effectively mixed by applying an AC signal with a peak voltage of 14 V and a frequency of 400 Hz. Figure 2a5, a6 exhibit the counter-rotating microvortexes on I–I cross-section and II–II cross-section. It is clear that the area of fluid interface is increased by the twisting and stretching of microvortices. The fluids closing to the edge of the microchannel are usually difficult to be well mixed in many micromixers as the poor fluid convection in these areas. Whereas the microvortices generated on the driving electrodes in our micromixer (shown in Fig. 2a5, a6) can drive these fluids to the midchannel. Then these fluids driven to the midchannel can be twisted and stretched by the ICEO microvortices. Therefore, the microvortices generated on the electrodes are also helpful to promote the mixing performance in this micromixer. Figure 2b, c shows the electric field intensity and the electroosmotic slip velocity across the y coordinate on I–I and II–II cross-section, respectively. Specifically, the electric field intensities and the ICEO slip velocities at the edge of electrodes are higher than that in other regions.

For the quantitative evaluation of mixing performance, the mixing index is defined as (Huang et al. 2007).

$$\text{Mixing index} = 1 - \frac{\sigma}{I_{av}} = \left(1 - \frac{\sqrt{1/n \sum (I_i - I_{av})^2}}{I_{av}}\right) \quad (10)$$

where I_i is the fluorescent intensity of each point, n is the number of pixels, and I_{av} is the average intensity over n pixels (in experiments, I_i and I_{av} are the fluorescent intensity of each point and the average intensity, respectively). For unmixed fluids, the mixing index is 0, as for the completely mixed fluids, the mixing index is 1. Usually the mixing index that is or above 0.9 indicates excellent mixing performance.

To make sure the credibility of simulation results, a grid-independence test was firstly carried out. Compared to the tetrahedral meshes, since the hexahedral meshes have better computational accuracy and faster convergence, the computational domain was completely covered

Table 1 The specific dimensions of the chip

Parameters	H	W_{cc}	W_{fc}	W_f	W	L_f	W_c	D_f	L_c
Value (μm)	38	120	100	50	120	500	170	25	3125

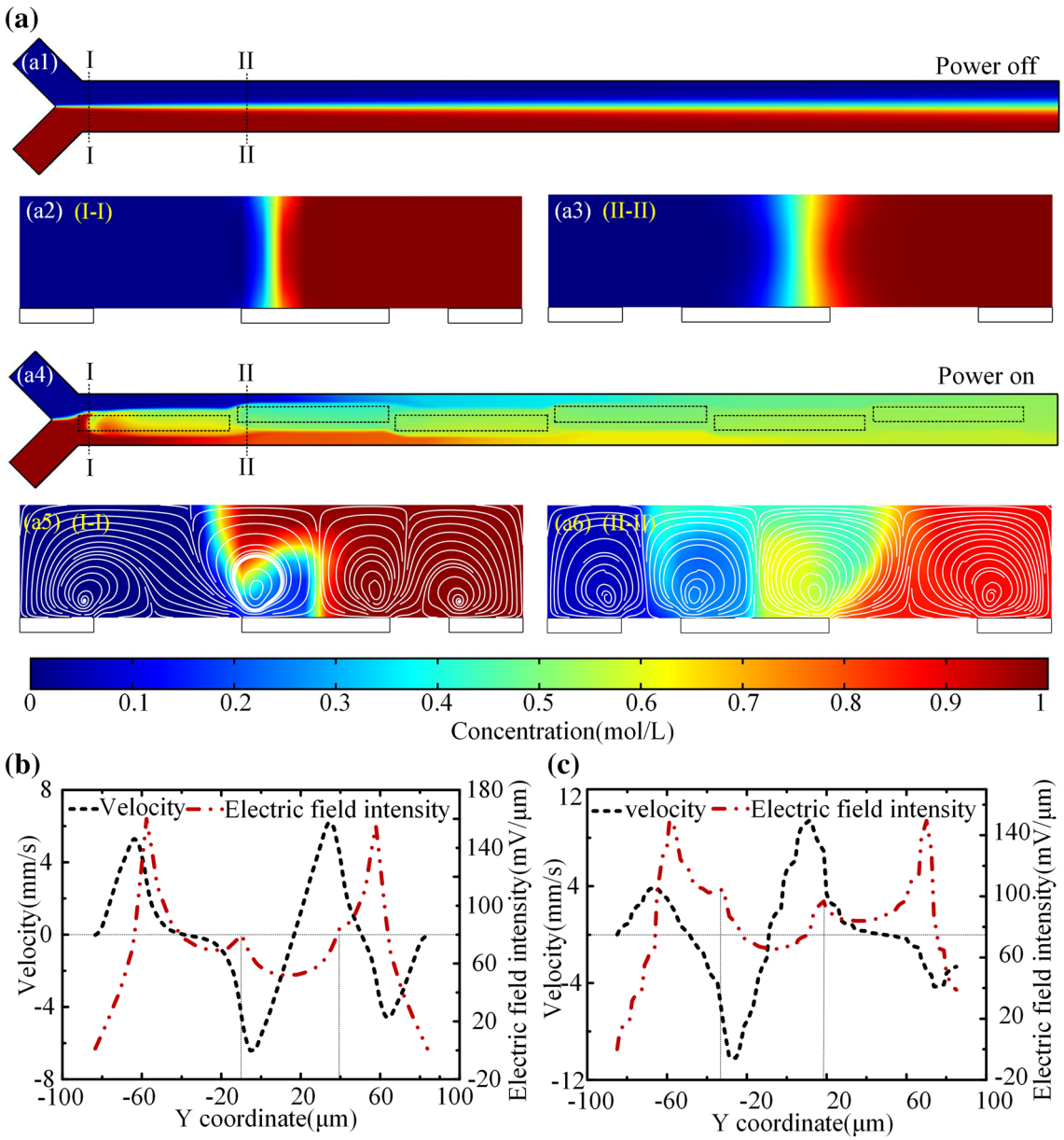

Fig. 2 **a** Simulation model of the micromixer, **a1**–**a3** shows the concentration state without an AC electric field, **a4** indicates concentration state at a flow rate of 1500 μm/s under a sinusoidal wave with a peak voltage of 14 V and a frequency of 400 Hz, **a5** shows the lateral motion state of fluids under the influence of the driving-electrode and the first floating-electrode. **a6** exhibits the lateral motion state of fluids under the influence of the driving-electrode and the second floating-electrode. **b** Velocity and electric field intensity across the *y* coordinate on I–I cross-section when *z* is 1 μm. **c** Velocity and electric field intensity across the *y* coordinate on II–II cross-section when *z* is 1 μm

by the hexahedral meshes. Eight simulation models with an element number ranging from 8.85×10^3 to 1.62×10^5 were simulated. The numerical results indicated that the influence of the number of elements on the simulation results can be neglected when the number of elements is above 8.62×10^4 (Fig. 3a). Thus, a simulation model with 8.62×10^4 hexahedral meshes is determined as the final model in terms of the accuracy and efficiency of simulation. The mixing profile shown in Fig. 3a indicates an efficient mixing performance at a flow rate of 1500 μm/s under an AC signal with a peak voltage of 14 V and a frequency of 400 Hz.

After the appropriate simulation model was established, we studied the influence of axial flow rate on the mixing performance (Fig. 3b). When the peak voltage is 10 V, we first determined the optimal frequency as 400 Hz by simulating the mixing performance under different frequencies ranging from 100 to 1000 Hz and axial velocities varying

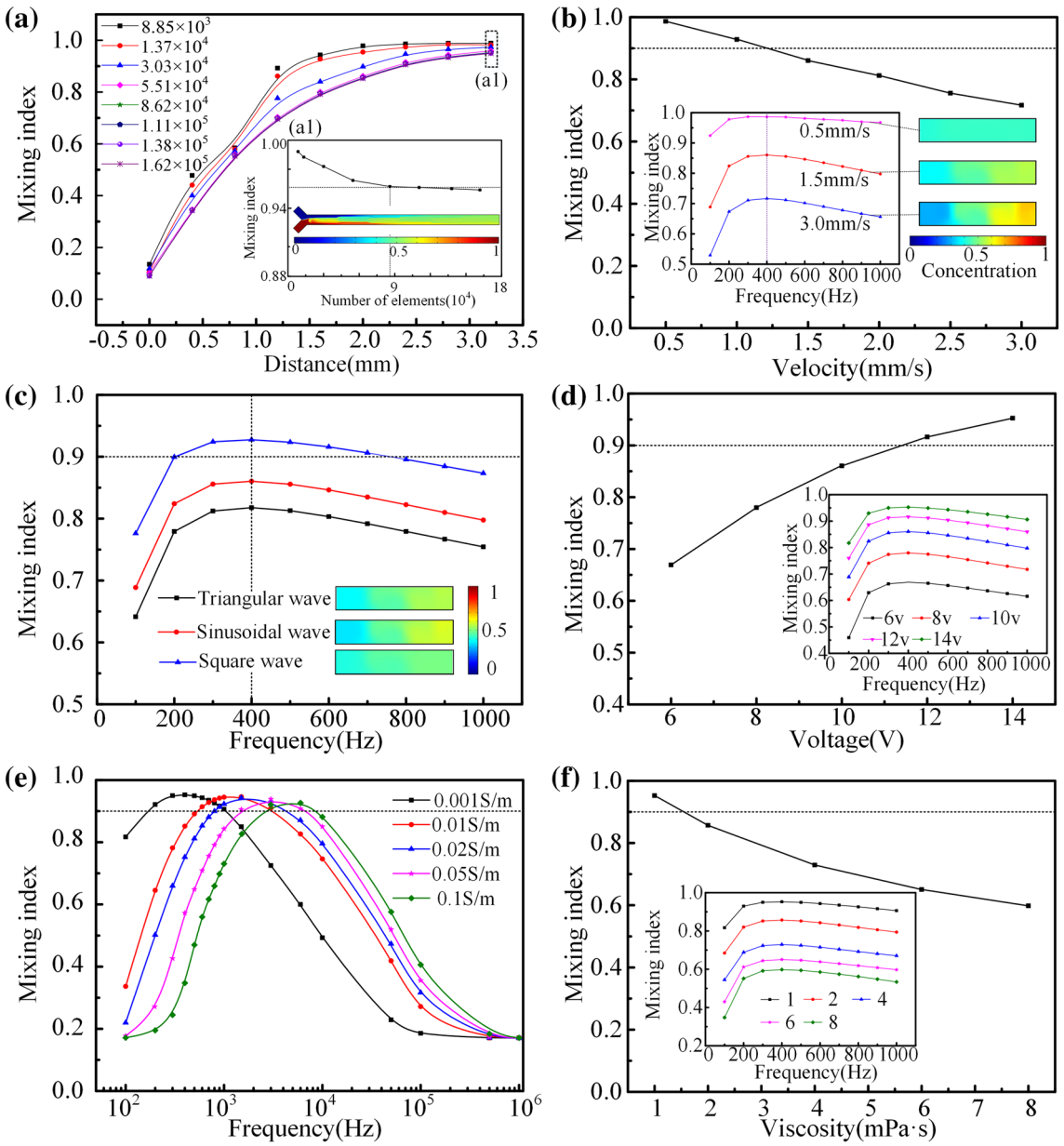

Fig. 3 **a** Mesh independency test of the simulation model (velocity is 1500 μm/s, sinusoidal wave, peak voltage is 14 V and frequency is 400 Hz). **b** Influence of fluid velocity on the mixing performance (sinusoidal wave, peak voltage is 10 V and the optimal frequency is 400 Hz). **c** A plot of the mixing performance versus the applied frequency when triangular wave, sinusoidal wave and square wave are applied on the driving electrodes (peak voltage is 10 V, velocity of fluid is 1500 μm/s). **d** Influence of the applied voltage on the mixing performance (velocity is 1500 μm/s, sinusoidal wave and optimal frequency is 400 Hz). **e** A plot of mixing performance versus the applied frequency for electrolytes with different conductivities (velocity is 1500 μm/s, sinusoidal wave and peak voltage is 14 V). **f** Influence of the viscosity of fluids on the mixing performance (velocity is 1500 μm/s, sinusoidal wave, peak voltage is 14 V and frequency is 400 Hz)

from 0.5 to 3.0 mm/s. Then we fitted a curve showing the relationship between the optimal mixing index and the axial flow rate (Fig. 3b). Clearly, the mixing efficiency decreases with the rising flow rates. This can be explained by the following statement. The fluids in microchannel flow both on the axial-section (driven by the axial pressure of fluids) and on the cross-section (driven by the applied AC electric field), the interface of two fluids can be effectively perturbed only when the axial flow velocity is close to the lateral velocity. With the rising axial flow rates, the interfacial perturbation caused by ICEO gradually decreases.

Then the dependence of mixing efficiency on the type of AC signal was investigated. When the peak voltage was 10 V, we simulated the mixing performances under different

frequencies and AC signals (Fig. 3c). The result in Fig. 3c shows that the optimal frequency is still 400 Hz and the micromixer has the best mixing performance when applying a square wave. According to the concentration distributions at the exit of the micromixer shown in Fig. 3c, we can conclude that the concentration distribution under a square wave is the most homogeneous. More importantly, when we use the square wave to replace the triangular wave, the mixing index can be increased from 81.7%, a general mixing state, to 92.8%, an effective mixed state. The reason why the micromixer under a square wave will have the best mixing performance is explained as follows. Based on Eq. (5), the ICEO slip velocity is proportional to the tangential electric field intensity ($\boldsymbol{E}_t$) and the potential difference of the double electric layer (ζ). The values of $\boldsymbol{E}_t$ and ζ are related to the time-averaged voltage of AC signals. Among triangular, sinusoidal and square wave, the square wave has the biggest time-averaged voltage when the frequency and the peak voltage of three kinds of AC signals are same. Therefore, the mixing performance can be effectively improved using square wave.

The voltage of applied AC signal can affect the potential difference of the electric double layer and the tangential electric field, therefore, we simulated mixing performances under a sinusoidal wave with different voltages ranging from 6 to 14 V. Figure 3d demonstrates that the mixing index increases with the increase of peak voltage. The mixing index can reach 95.3% when applying a sinusoidal wave with a frequency of 400 Hz and a peak voltage of 14 V.

Furthermore, we simulated the mixing performance under different solution conductivities ranging from 0.001 to 0.1 S/m. According to Fig. 3e, the optimal frequency increases with the rising solution conductivities, but the optimal mixing index decreases with the increase of solution conductivity. This phenomenon can be explained by the basic ICEO theory. The optimal frequency of AC signal $f_c = (1+\delta)\sqrt{D\varepsilon\sigma}/(2\pi\varepsilon L)$ increases with the increasing solution conductivities. As for the thickness of the electric double layer $\lambda_D = \sqrt{D\varepsilon/\sigma}$, it decreases as the solution conductivity increases. The fluids out of the electric double layer are driven by viscous force provided by the fluids in the electric double layer. When the electric double layer is too thin, the charged-fluids in the electric double layer will not be able to drive the fluids out of the double layer to move. Therefore, the optimal mixing index decreases with the increase of solution conductivity.

Finally, we numerically analyzed the influence of fluid viscosity on the mixing performance (Fig. 3f). When the axial velocity and the peak voltage of the sinusoidal wave is 1500 μm/s and 14 V, respectively, the optimal frequency is still 400 Hz by investigating the mixing performances under different frequencies ranging from 100 to 1000 Hz. The fitted curve in Fig. 3f shows that the fluid viscosity has a negative effect on the mixing performance. Specifically, the mixing index decreases from 92.8 to 60% when the fluid viscosity rises from 1 to 8 mPa s. This phenomenon can be explained by Eq. (5), that is, at higher viscosity of fluids, the interfacial perturbation effect tends to be weaker.

4.2 Experimental results

For demonstrating the efficient mixing performance of this micromixer, except for a series of simulations, we also conducted systematically experiments by injecting the undyed KCl solution and the fluorescent one into the microchannel through two separate inlets. Figure 4 shows some typical fluorescent profiles in the micromixer. Figure 4a indicates the unmixed laminar flow state at a flow rate of 1500 μm/s with the power off, in which a clear interface was observed. Figure 4b–d exhibit the mixing results when the voltage and the frequencies of the applied AC signal are 14 V, 300 Hz; 14 V, 400 Hz; and 14 V, 500 Hz, respectively. Clearly, the normalized concentration of the unmixed laminar flow is the most inhomogeneous (Fig. 4e). The distribution of normalized concentration at 400 Hz is the most homogeneous (Fig. 4e).

We first experimentally studied the influence of fluid velocity on the mixing performance. Figure 5a indicates that

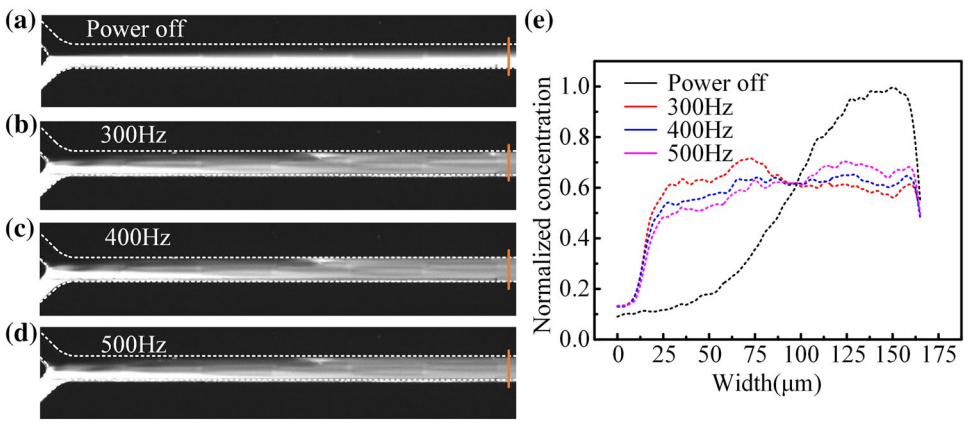

Fig. 4 **a–d** Concentration distribution profiles under different frequencies. (Velocity is 1500 μm/s and the peak voltage is 14 V). **e** Plots of normalized fluorescent concentration across the width of channel

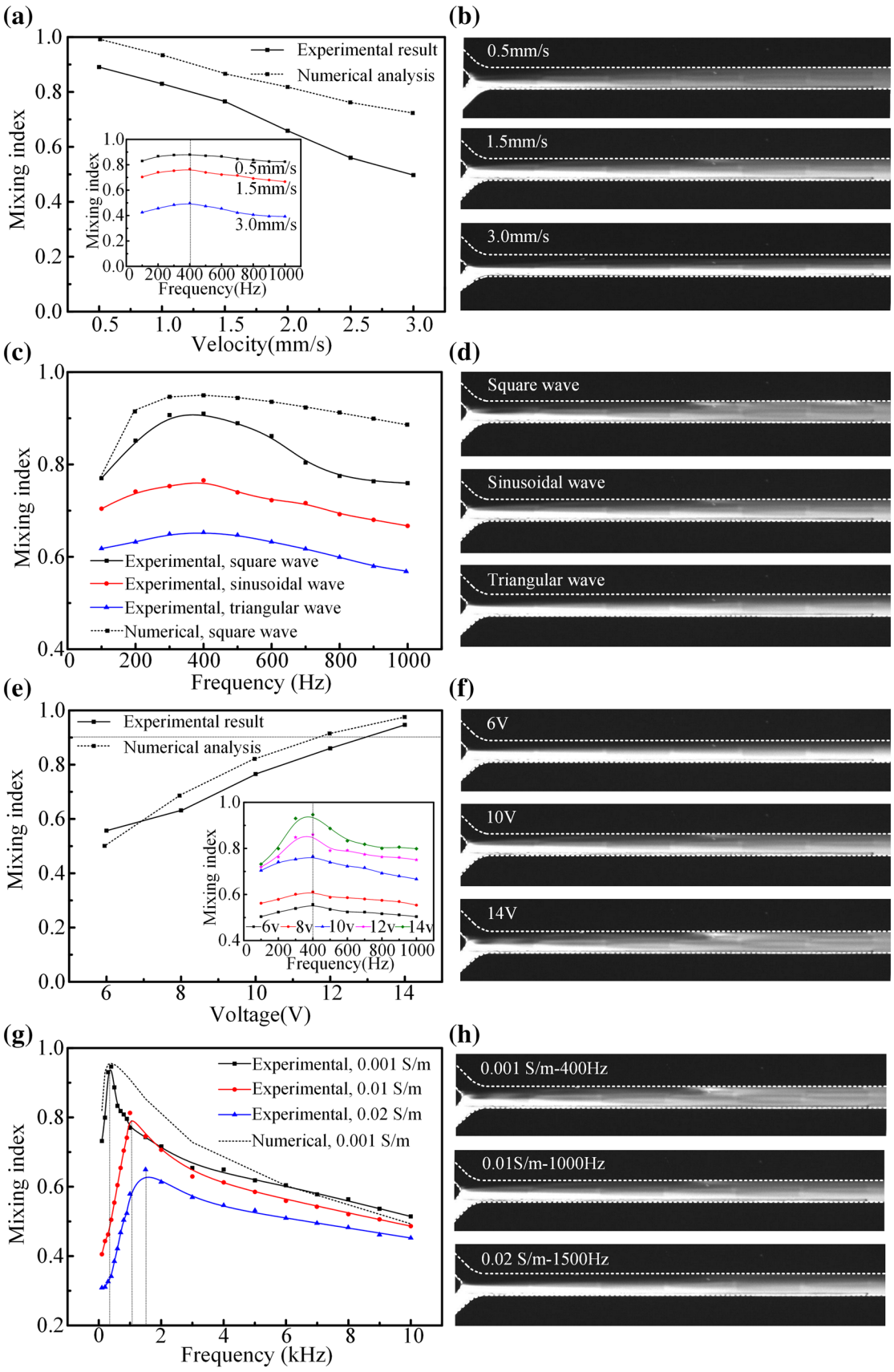
(a)
Experimental result
Numerical analysis
Mixing index
Velocity(mm/s)
0.5mm/s
1.5mm/s
3.0mm/s
Frequency(Hz)
(b)
0.5mm/s
1.5mm/s
3.0mm/s
(c)
Experimental, square wave
Experimental, sinusoidal wave
Experimental, triangular wave
Numerical, square wave
Mixing index
Frequency (Hz)
(d)
Square wave
Sinusoidal wave
Triangular wave
(e)
Experimental result
Numerical analysis
Mixing index
Voltage(V)
6v 8v 10v 12v 14v
Frequency(Hz)
(f)
6V
10V
14V
(g)
Experimental, 0.001 S/m
Experimental, 0.01 S/m
Experimental, 0.02 S/m
Numerical, 0.001 S/m
Mixing index
Frequency (kHz)
(h)
0.001 S/m-400Hz
0.01S/m-1000Hz
0.02 S/m-1500Hz

◂**Fig. 5** **a, b** Influence of fluid velocity on mixing performance. **c, d** Mixing performance versus the applied frequency under different signals. **e, f** Effect of the peak voltage on mixing performance. **g, h** Influence of the solution conductivity on the mixing efficiency (see Movie S1)

the mixing performance decreases from 0.9 to 0.5 as the fluid velocity rises from 0.5 to 3 mm/s at 10 V and 400 Hz. The optimal frequency, 400 Hz, is determined by analyzing the mixing efficiencies under different frequencies ranging from 100 to 1000 Hz. Comparing the experimental result to the numerical analysis, although they have same variation trend, the experimental values are a bit smaller than that in simulations. The reason is that the unspecific adhesion of the fluorescence particle on the channel walls causes uneven distribution of normalized fluorescent intensity. Figure 5b shows the mixing profiles under the flow rate of 0.5 mm/s, 1.5 mm/s and 3 mm/s at 10 V and 400 Hz. The mixing profiles clearly indicate the dependence of mixing performance on fluid velocity (also see supporting information).

Then the influence of the type of AC signal on mixing performance was analyzed. Figure 5c shows the mixing performance versus the applied frequency under triangular wave, sinusoidal wave and square wave. This micromixer exhibits the best mixing performance of 90.98% under a square wave with a peak voltage of 10 V and a frequency of 400 Hz. The reason is that the square wave has the best time-averaged voltage causing the biggest electroosmotic slip velocity when the peak voltage and the frequency of three kinds of AC signals are same. Due to the existence of oxide layer of ITO, buffer capacitance and surface conduction, the practical ICEO slip velocity is lower than the theoretical value. Therefore, the mixing performances obtained by experiments are a bit worse than that in simulations (The comparisons under other signals are given in Fig. S1). The mixing profiles at different AC signals are shown in Fig. 5d (see Support Information), it is clear that the distribution of fluorescence under the square wave is the most homogeneous.

Apart from the type of AC signal, we studied the effect of the peak voltage on mixing performance. Figure 5e indicates that the mixing performance apparently increases with the rising voltages when the fluid velocity is 1500 μm/s, the frequency of the AC signal is 400 Hz. The optimal frequency is determined by analyzing the mixing efficiencies under different frequencies. More importantly, the mixing performance of the micromixer can reach a perfect mixing state, 94.7%, at 14 V. The mixing profiles under different voltages shown in Fig. 5f clearly exhibit the effect of the voltage on the mixing performance (see supplementary information).

Furthermore, we performed the mixing experiments under different solution conductivities. Figure 5g shows that the mixing index apparently decreases with the rising solution conductivities. Comparing the experimental result to the simulation at 0.001 S/m, although they have same variation trend, the mixing index in experiment is obviously lower than that in numerical analysis (The comparisons under other solution conductivities are shown in Fig. S2). This phenomenon can be explained by the existence of oxide layer of ITO, the buffer capacitance and the surface conduction in experiments. Specifically, numerical analysis usually does not consider the influences of these items on mixing performance, but they would definitely decrease the ICEO slip velocity. The decreased slip velocity then causes the decrease of mixing efficiency. The mixing profiles under different solution conductivities shown in Fig. 5h clearly exhibit the negative effect of the solution conductivity on the mixing performance. Therefore, this experiment demonstrates that this micromixer is efficient for manipulating low conductive solutions.

Finally, we compared this micromixer with different micromixing devices using a comparative mixing index (CMI). Usually, the mixing index is obtained at the channel outlet by evaluating the standard deviation of gray-value at the exit. Whereas this method does not consider the variation of samples residence time among different designs. Jain et al. (2010) proposed a comparative mixing index (CMI) accommodating the residence time to judge the non-diffusive mixing enhancement for various micromixers over the T-mixer. The CMI is defined by the following equation:

$$\mathrm{CMI}_{\mathrm{X,T}} = \frac{(\mathrm{Me})_{\mathrm{X}}|_{(L_c,\tau)}}{(\mathrm{Me})_{\mathrm{T}}|_{(L_c,\tau)}} \tag{11}$$

where $(\mathrm{Me})_{\mathrm{X}}$ is the mixing efficiency of an arbitrary micromixer; $(\mathrm{Me})_{\mathrm{T}}$ is the mixing efficiency of the T-mixer [the channel structure of a T-mixer is defined by Tafti et al. (2008)].

The theoretical limits for CMI is between one and infinity. And it can be used to evaluate any arbitrary designs by benchmarking the mixing efficiency with respect to T-mixers for same residence time. When the micromixer with different channel lengths are compared under different flow rates, the non-diffusive mixing improvement can be obtained by normalizing the effect of residence time. Thus, it would be reasonable and useful to compare various micromixer designs using the CMI. According to the CMI, the mixing performance of our micromixer was evaluated by comparing it to the micromixer with coplanar electrodes based on DC-biased ACEO flow, the Sigma micromixer and the micromixer with Tesla structures (Table 2).

According to Table 2, the non-diffusive mixing improvement of our micromixer reaches up to 316%, which is the highest value among these mixing devices. Therefore, this presented micromixer remains competitive among these existing designs. What's more, the current micromixer (a)

Table 2 Comparison of mixing performance of (a) the proposed micromixer, (b) micromixer with coplanar electrodes based on DC-biased ACEO flow (Ng et al. 2009) (c) sigma micromixer (Hong et al. 2004), (d) micromixer with Tesla structures (Tafti et al. 2008)

Micromixers	L (mm)	$(Me)_T$ (%)	Me (%)	CMI
(a)	3.2	30	94.7	3.16
(b)	0.6	31	92	2.96
(c)	17	46	80	1.7
(d)	17	46	62	1.37

is much easier to fabricate in comparison with other ICEO-based micromixers which always need an array of complicated conducting-posts with various shapes and arrangements in microchannels. Therefore, this design can offer a simple method for improving the fluid mixing performance.

5 Conclusions

In this work, we demonstrated the mixing capability of an ICEO-based micromixer. The current device utilizes simple planar asymmetrical floating electrodes made of ITO glass to generate effective microvortices crossing the fluidic interface. The mixing efficiency was thoroughly investigated by simulations and experiments, showing that the mixing efficiency can reach 94.7% within 3.2 mm mixing length under a sinusoidal wave with a peak voltage of 14 V and a frequency of 400 Hz when the axial flow rate is 1500 μm/s. The mixing performance of the proposed micromixer was also appropriately compared with some other micromixers using the comparative mixing index (CMI), demonstrating that this micromixer remains competitive among these existing designs. The current micromixer is expected to have advantages such as simple structure, low cost, flexible manipulation, and robust and stable performance. Therefore, this work provides a promising approach for efficient electrokinetic mixing with broad applications in microfluidic systems.

Acknowledgements This work was financially supported by the National Natural Science Foundation of China (Grant no. 11672095, no. 11702035 and no. 11702075), the Foundation for Innovative Research Groups of the National Natural Science Foundation of China (Grant no. 51521003), and the Opening fund of State Key Laboratory of Nonlinear Mechanics. We are also grateful to Haizhen Sun, Mingyu Xiao, Yupan Wu and Weiyu Liu for their assistance in the simulation and helpful results discussions.

References

Alipanahrostami M, Ramiar A (2017) High efficiency micromixing technique using periodic induced charge electroosmotic flow: a numerical study. Colloids Surf A Physicochem Eng Asp 524:53–65

Chang C-C, Yang R-J (2007) Electrokinetic mixing in microfluidic systems. Microfluid Nanofluid 3:501–525. https://doi.org/10.1007/s10404-007-0178-z

Chen JK, Yang RJ (2007) Electroosmotic flow mixing in zigzag microchannels. Electrophoresis 28:975–983. https://doi.org/10.1002/elps.200600470

Chiu P-H, Chang C-C, Yang R-J (2012) Electrokinetic micromixing of charged and non-charged samples near nano-microchannel junction. Microfluid Nanofluid 14:839–844. https://doi.org/10.1007/s10404-012-1116-2

Daghighi Y, Li D (2013) Numerical study of a novel induced-charge electrokinetic micro-mixer. Anal Chim Acta 763:28–37

Feng X, Ren Y, Jiang H (2013) An effective splitting-and-recombination micromixer with self-rotated contact surface for wide Reynolds number range applications. Biomicrofluidics 7:54121

Feng X, Ren Y, Jiang H (2014) Effect of the crossing-structure sequence on mixing performance within three-dimensional micromixers. Biomicrofluidics 8:412

Gorkin R et al (2010) Centrifugal microfluidics for biomedical applications. Lab Chip 10:1758

Harnett CK, Templeton J, Dunphyguzman KA, Senousy YM, Kanouff MP (2008) Model based design of a microfluidic mixer driven by induced charge electroosmosis. Lab Chip 8:565–572

Hong CC, Choi JW, Ahn CH (2004) A novel in-plane passive microfluidic mixer with modified Tesla structures. Lab Chip 4:109–113

Huang SH, Wang SK, Khoo HS, Tseng FG (2007) AC electroosmotic generated in-plane microvortices for stationary or continuous fluid mixing. Sens Actuators B Chem 125:326–336

Ickmans K et al (2013) Association between cognitive performance, physical fitness, and physical activity level in women with chronic fatigue syndrome. J Rehabil Res Dev 50:795

Jain M, Yeung A, Nandakumar K (2009) Induced charge electro osmotic mixer: obstacle shape optimization. Biomicrofluidics 3:368

Jain M, Yeung A, Nandakumar K (2010) Analysis of electrokinetic mixing techniques using comparative. Mixing Index Micromach 1:36–47

Jegatheeswaran S, Ein-Mozaffari F, Wu J (2017) Efficient mixing of yield-pseudoplastic fluids at low Reynolds numbers in the chaotic SMX static mixer. Chem Eng J 317:215–231

Johansson L, Johansson S, Nikolajeff F, Thorslund S (2009) Effective mixing of laminar flows at a density interface by an integrated ultrasonic transducer. Lab Chip 9:297

Kai Z, Mi XJ, Yu MZ (2012) Design of super-efficient mixer based on induced charge electroosmotic. Therm Sci 16:1534–1538

Liu W, Ren Y, Tao Y, Yao B, Liu N, Wu Q (2017) A universal design of field-effect-tunable microfluidic ion diode based on a gating cation-exchange nanoporous membrane. Phys Fluids 29:112001

Lu X et al (2013) Detecting and tracking nosocomial methicillin-resistant staphylococcus aureus using a microfluidic SERS. Biosens Anal Chem 85:2320

Matsubara K, Narumi T (2016) Microfluidic mixing using unsteady electroosmotic vortices produced by a staggered array of electrodes. Chem Eng J 288:638–647

Ng WY, Goh S, Lam YC, Yang C, Rodríguez I (2009) DC-biased AC-electroosmotic and AC-electrothermal flow mixing in microchannels. Lab Chip 9:802–809

Ozcelik A, Ahmed D, Xie Y, Nama N, Qu Z, Nawaz AA, Huang TJ (2014) An acoustofluidic micromixer via bubble inception and cavitation from microchannel sidewalls. Anal Chem 86:5083–5088. https://doi.org/10.1021/ac5007798

Ren Y et al (2017) Flexible particle flow-focusing in microchannel driven by droplet-directed induced-charge electroosmosis. Electrophoresis 39:597–607

Sasaki N, Kitamori T, Kim H-B (2006) AC electroosmotic micromixer for chemical processing in a microchannel. Lab Chip 6:550–554. https://doi.org/10.1039/B515852D

Tafti EY, Kumar R, Cho HJ (2008) Effect of laminar velocity profile variation on mixing in microfluidic devices: the sigma micromixer. Appl Phys Lett 93:190

Wu Z, Li D (2008) Micromixing using induced-charge electrokinetic flow. Electrochim Acta 53:5827–5835

Wu Y, Ren Y, Tao Y, Hou L, Hu Q, Jiang H (2016) A novel micromixer based on the alternating current-flow field effect transistor. Lab Chip 17:186

Wu Y, Ren Y, Jiang H (2017) Enhanced model-based design of a high-throughput three dimensional micromixer driven by alternating-current electrothermal flow. Electrophoresis 38:258–269

Xia HM, Wan SY, Shu C, Chew YT (2005) Chaotic micromixers using two-layer crossing channels to exhibit fast mixing at low Reynolds numbers. Lab Chip 5:748

Xia HM, Wang ZP, Koh YX, May KT (2010) A microfluidic mixer with self-excited 'turbulent' fluid motion for wide viscosity ratio applications. Lab Chip 10:1712

Xie Y, Ahmed D, Lapsley MI, Lin S-CS, Nawaz AA, Wang L, Huang TJ (2012) Single-shot characterization of enzymatic reaction constants K_m and k_{cat} by an acoustic-driven bubble-based fast micromixer. Anal Chem 84:7495–7501. https://doi.org/10.1021/ac301590y

Yasui T et al (2011) Microfluidic baker's transformation device for three-dimensional rapid mixing. Lab Chip 11:3356–3360

Ye LJ, Li YM, Zhang AL (2009) Fast mixing digital micro-fluids in PDMS microchannel based on surface acoustic wave. In: Symposium on Piezoelectricity, Acoustic waves, and Device applications. IEEE, pp 19–23

Yesiloz G, Boybay MS, Ren CL (2017) Effective thermo-capillary mixing in droplet microfluidics integrated with a microwave heater. Anal Chem 89:1978–1984. https://doi.org/10.1021/acs.analchem.6b04520

Zhao H, Bau HH (2007) Microfluidic chaotic stirrer utilizing induced-charge electro-osmosis. Phys Rev E 75:066217

Zhou B et al (2015) Design and fabrication of magnetically functionalized flexible micropillar arrays for rapid and controllable microfluidic mixing. Lab Chip 15:2125–2132

Zhu GP, Nguyen NT (2012) Rapid magnetofluidic mixing in a uniform magnetic field. Lab Chip 12:4772